Electrochemical Characterization of Dopamine in Neural Cells With Flexible Biosensors

Mehran Abbasi Shirsavar
Department of Mechanical Engineering,
Iowa State University,
Ames, IA 50011
e-mail: mehran@iastate.edu

Amir Niaraki
Department of Mechanical Engineering,
Iowa State University,
Ames, IA 50011
e-mail: niaraki@iastate.edu

Nicole N. Hashemi[1]
Department of Mechanical Engineering,
Iowa State University,
Ames, IA 50011;
Department of Mechanical Engineering,
Stanford University,
Stanford, CA 94305
e-mails: nastaran@iastate.edu;
nicolenh@stanford.edu

Dopamine is critical for the physiological function and plays a crucial role in the discovery of neurological disorders such as Parkinson's disease. Improving the measurement of this neurotransmitter could improve treatment, diagnosis, and prognosis of neurological disorders. Graphene's outstanding biocompatibility and electrical conductivity have caused it to become a widely used material in cellular interfacing and neurotransmitter characterization. However, graphene has been rarely used to investigate cellular systems after introducing trauma. Sensing dopamine on the cellular level and on the microscale can lead to provide a point-of-care diagnostics for traumatic brain injury patients. The sensitivity of graphene biosensor to different concentrations of dopamine was evaluated in the dynamic range of 0.1–100 μM, and the limit of detection of biosensor was estimated to be 180 μM. In this work, a 3D-printed graphene biosensor was used to characterize the dopamine levels as a real-time detector of neurotransmitters. We used cyclic voltammetry (CV) to measure the response of graphene biosensors to neurotransmitter changes, in addition, to evaluate the effect of UV irradiation as the injury stimulant on the electrical properties of graphene biosensors. We demonstrated that the 3D-printed graphene could detect significant changes in the CV profiles of N27 dopaminergic neural cells cultured on the graphene device in the face of trauma. [DOI: 10.1115/1.4054417]

Keywords: graphene, traumatic brain injury, dopamine, electrochemistry, biocompatibility, additive manufacturing, biomedical manufacturing, sensors, monitoring and diagnostics

1 Introduction

The neurotransmitter dopamine is crucial for physiological and neurological functions [1–4]. Insufficient production of dopamine can lead to Parkinson's disease, schizophrenia, and attention deficit hyperactive disorder [1–5]. The anatomic properties of dopaminergic systems can cause traumatic brain injuries (TBIs) as a major reason for death and disability [5].

Therefore, the quantification and detection of dopamine can play an important role in understanding the aforementioned brain disorders. Some studies have shown that dopamine levels were disrupted in TBI cases [6–8], but it remains to translate this knowledge into patient care and treatment. Hence, the fabrication of precise methods for dopamine detection is the focus of many studies [9–12]. Kujawska et al. [13] applied graphene biosensor for dopamine detection showed a good selectivity and sensitivity with a limit of detection of 1–1.5 μM. Hou et al. [14] chemically modified the graphene surface via silanization to include carboxylic groups on graphene–Nafion electrodes. The modified graphene showed a good selectivity in detecting dopamine, and the cyclic voltammetry (CV) results exhibited a reversible oxidation behavior of dopamine at the interface of graphene electrodes. Qi et al. [15] fabricated an electrochemical sensor using pristine graphene using liquid-phase exfoliation of graphite. This sensor was able to detect ascorbic acid, dopamine (DA), and uric acid with detection limits of 6.45, 2.00, and 4.82 μM, respectively.

Traditional techniques of measuring dopamine levels have included mass spectrometry coupled with separation techniques such as chromatography, optical methods such as fluorescence, and chemiluminescence-based methods. However, such techniques suffer from requiring complex protocols, complex training, and expensive equipment, although they are highly selective and sensitive [1].

More recent methods have focused on electrochemical characterizations and measurements with advantages such as low cost, quick response, and ease of use [3,16,17]. Choo et al. [18] used 3D-porous graphene oxide (pGO)/gold nanoparticle/pGO composite-modified indium tin oxide to detect dopamine using an electrochemical method.

Microfluidic-based techniques like lab-on-a-chip and microfiber applications have also become widespread and gained attention for investigating public health issues and alternative energy sources due to the economics and efficiency of experimenting on the microscale [19–29]. Real-time quantification and sensitive measuring of dopamine can improve the diagnosis and treatment methods [1]. Manbohi and Ahmadi [30] applied their microfluidic nanosensor in detecting dopamine in blood and urine samples using a mixture of graphite, chitosan, and poly ethylene glycol in a three-electrode system.

The performance of sensor in detection of different concentrations of dopamine was evaluated using fluorescence spectra luminescent graphene quantum dots in a label-free method. The results showed that decreasing the dopamine concentrations increased the fluorescence intensity [31].

A promising material in the investigation of dopamine concentration and postsynaptic potentials [4] is graphene [32–35]. This is due to its excellent biocompatibility with different biomolecules like DNA, cells, enzymes, and proteins, as well as outstanding electrical conductivity. Graphene electrodes can be used in electrochemical characterizations such as cyclic voltammetry and to enhance dopamine oxidation [36–38]. Suzuki et al. used carbon nanotubes to determine action potentials, post synaptic potentials, and dopamine concentration using amperometry and differential pulse voltammetry [4]. Emran et al. [39] studied the dopaminergic PC12 cell line to monitor the dopamine level using amperometric response of the cells in 0.1 M phosphate-buffered saline (PBS). The amperometric addition of dopamine source showed a fast response, and the

[1]Corresponding author.

Manuscript received January 18, 2022; final manuscript received April 16, 2022; published online May 19, 2022. Assoc. Editor: Robert Chang.

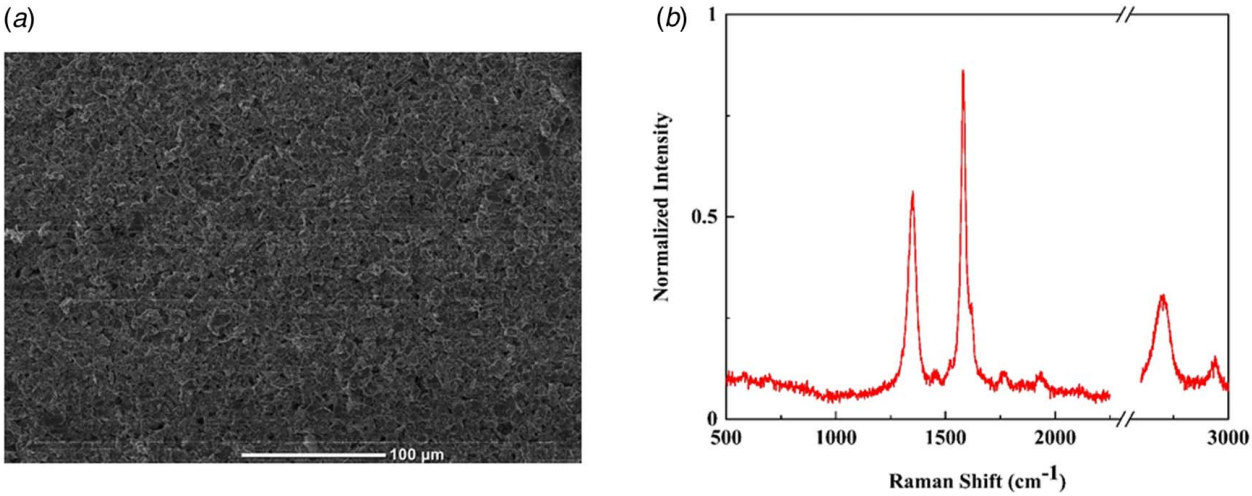

Fig. 1 (*a*) SEM images of the surface of E-jet-printed graphene electrodes and (*b*) Raman spectrum of graphene collected at $\lambda = 532$ nm to estimate the lattice defects on graphene

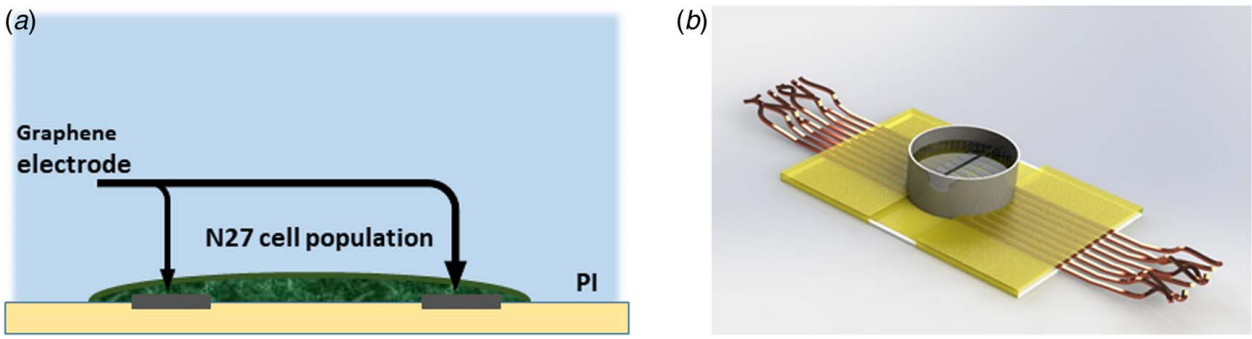

Fig. 2 (*a*) Schematic of biosensor shows the interface of graphene electrodes and N27 cells to measure the electrical properties of biosensors by connecting the electrodes to Potentiostat and (*b*) PDMS was used to mount a well on graphene electrodes and confine the interaction of cell lines with electrodes

incubation of cells in KCl for 30 min increased the peak current significantly. Lan et al. used glassy carbon electrodes modified with graphene oxide to quantify the dopamine using anodic peak voltammetry and CV for characterization of the device [5]. However, Hassine et al. used graphene oxide, which is insulating, and oxidation may not be desired in some cases [3,40]. As oxidation plays a major role in electrochemical characterization methods widely used to measure dopamine, this may not be desirable.

In this study, we use 3D-printed, mechanically exfoliated graphene systems to quantify and characterize dopamine activities with the graphene being the only electrode. We then used N27 dopaminergic neurons to access the dopamine. Cyclic voltammetry was used for the characterization of the device and measurement of dopamine levels in prepared dopamine solutions. This work can provide a point-of-care diagnostics for traumatic brain injury patients.

2 Experimental Section

2.1 Graphene Production. Graphite crystallites (synthetic graphite powder ~20 μM, Aldrich Chemistry, St. Louis, MO) and bovine serum albumin (BSA; A7906, Sigma-Aldrich, St. Louis, MO) were broken down into few layer graphene (FLG) platelets by the abrasion of steel balls with a diameter of 0.3438 in.

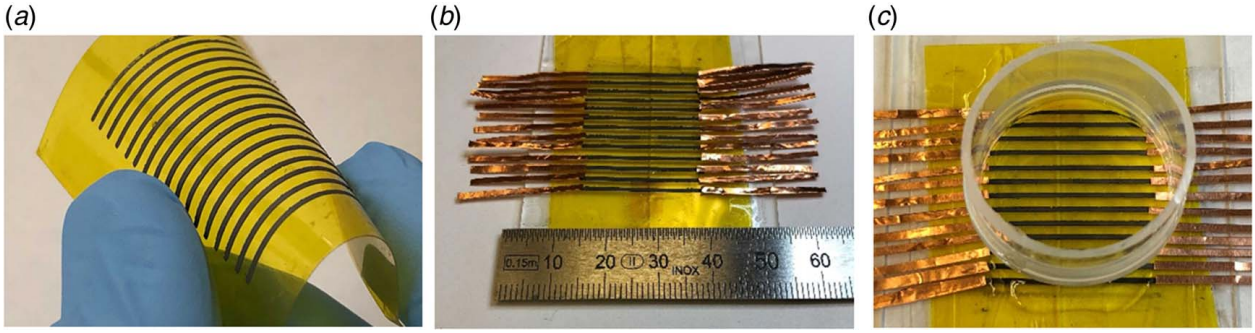

Fig. 3 The development of the device and the different stages of manufacturing: (*a*) flexibility of inkjet-printed graphene electrodes, (*b*) attachment of copper tape and silver paste to electrodes prior to electrochemical measurements, and (*c*) the cell culture canister has been affixed using epoxy and PDMS

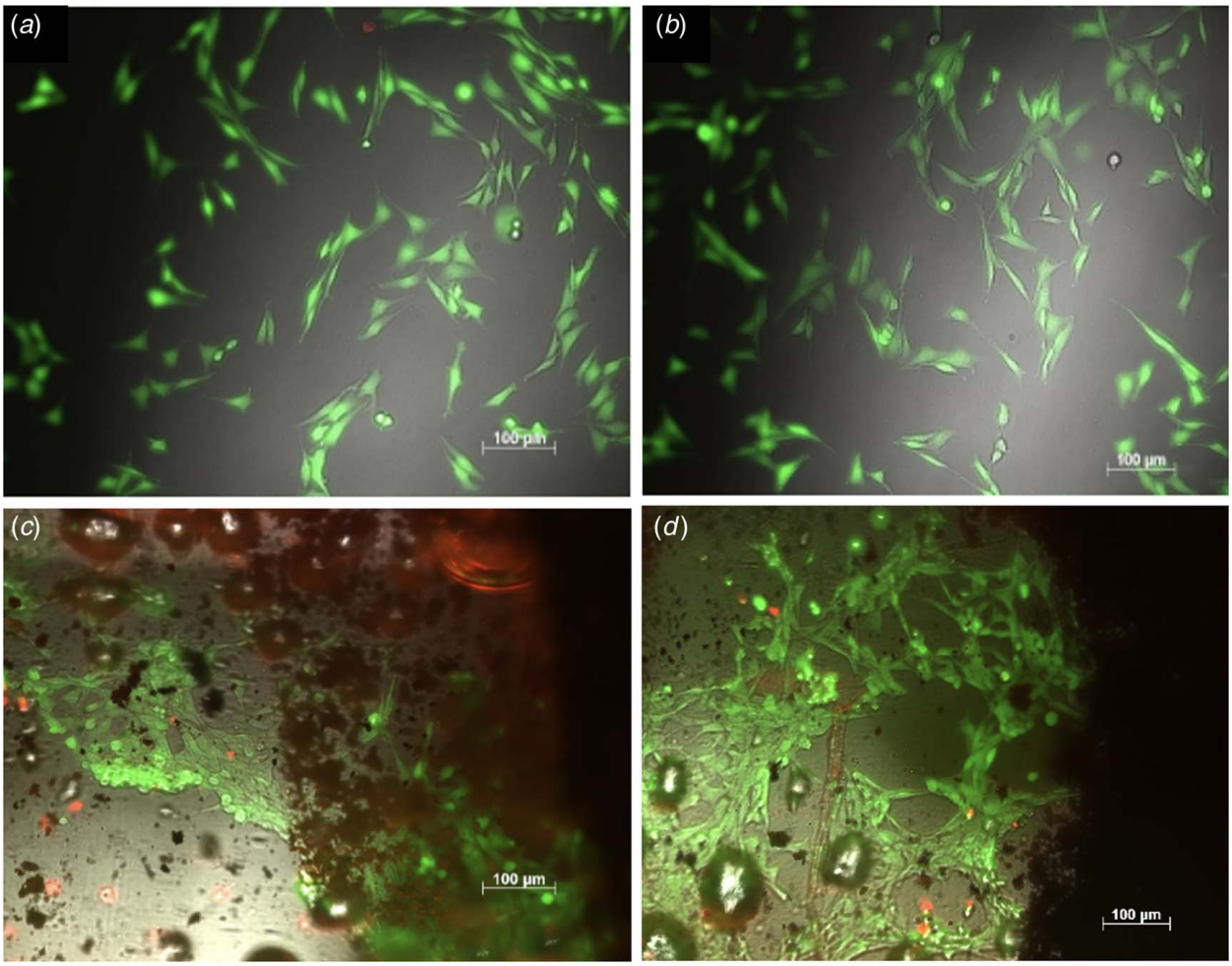

Fig. 4 (*a*) and (*b*) Control live-dead cell assay, and (*c*) and (*d*) N27 dopaminergic cells shown 24 h after being interfaced with 3D-printed graphene sensors and stained using CellTracker™ Green CMFDA and propidium iodide. Scale bars indicate 100 μm.

[19,40,41]. As turbulent energy dissipation is not necessary for exfoliation, the rotational speed was set at 300 rpm for 90 h in all trials to prevent undesired temperature spikes [40]. The proportions of graphite (20 mg/ml) and BSA (2 mg/ml) were constant throughout this study. BSA was used to stabilize the resulting solution. r_{ibs} here represents the ratio of the overall surface area of the balls with respect to the solution volume [19]. The ball-milled solution was allowed to rest for 48 h. As not all graphite particles can be exfoliated to the desired FLG state, it is necessary to remove the thicker graphene sheets that failed to bond with BSA. To do this, the solution was centrifuged further at 1500 rpm for 45 min. Eighty-five percent of the volume was pipetted off from the top of the solution [40].

2.2 3D-Printed Graphene Chip Manufacturing. Graphite was purchased from Aldrich Chemical Company, St. Louis, MO. Electrically conductive Copper tape was obtained from Electron Microscopy Sciences, Hatfield, PA. Conductive silver paste was obtained from Ted Pella Inc., Redding, CA. Polydimethylsiloxane (PDMS) elastomer curing kit was obtained from Dow Corning, Midland, MI. Kapton polyimide was purchased from Sigma-Aldrich. Polyimide (PI) has a hydrophobic surface and requires surface modification to make the substrate compatible with the aqueous graphene ink. The surface modification process started with washing PI film using deionized (DI) water and acetone before plasma cleaning, and then, it was submerged in a solution of poly 4-styrenesulfonic acid sodium salt in DI water at a concentration of 12 mg/ml and NaCl at a concentration of 0.5 M for 20 min followed by submergence in a solution of poly ethyleneimine in DI water at a concentration of 30 mg/ml and NaCl at a concentration of 0.5 M for 20 min.

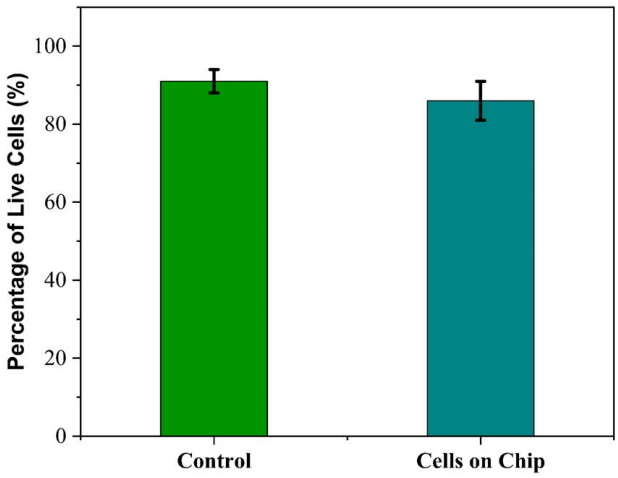

Fig. 5 Cell viability of the device is shown to be 85% (the percentage of live cells is 85% by interfacing the cells on graphene biosensors) (tests were repeated for three sensors)

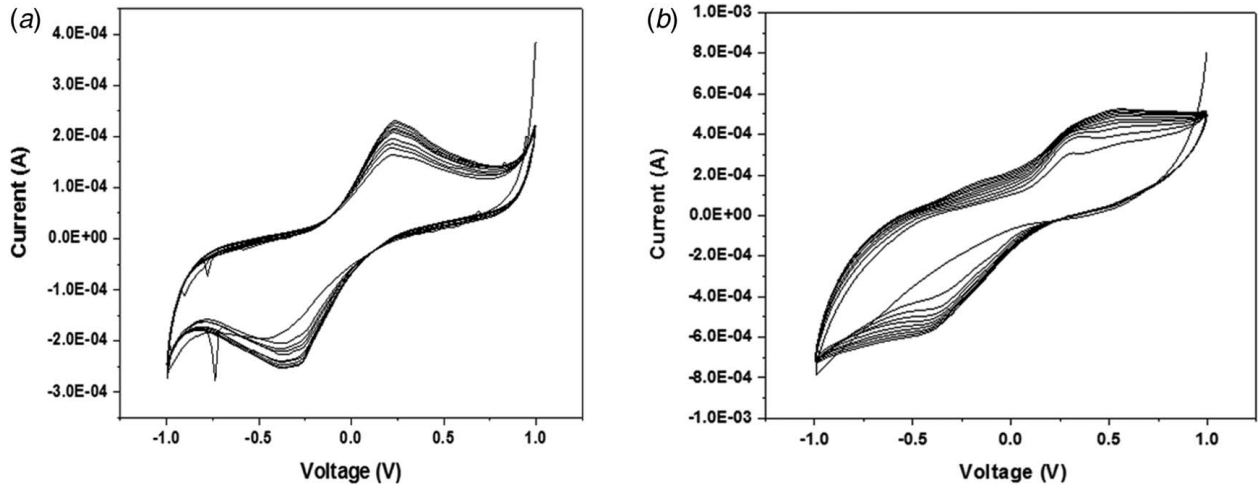

Fig. 6 CV characterization of the 3D-printed graphene device: (*a*) CV profile of 0.001 M DA in 0.1_M PBS using the 3D-printed graphene device as the electrode and (*b*) CV profile of 0.001 M DA in 0.1 M PBS using a second 3D-printed graphene device as the electrode

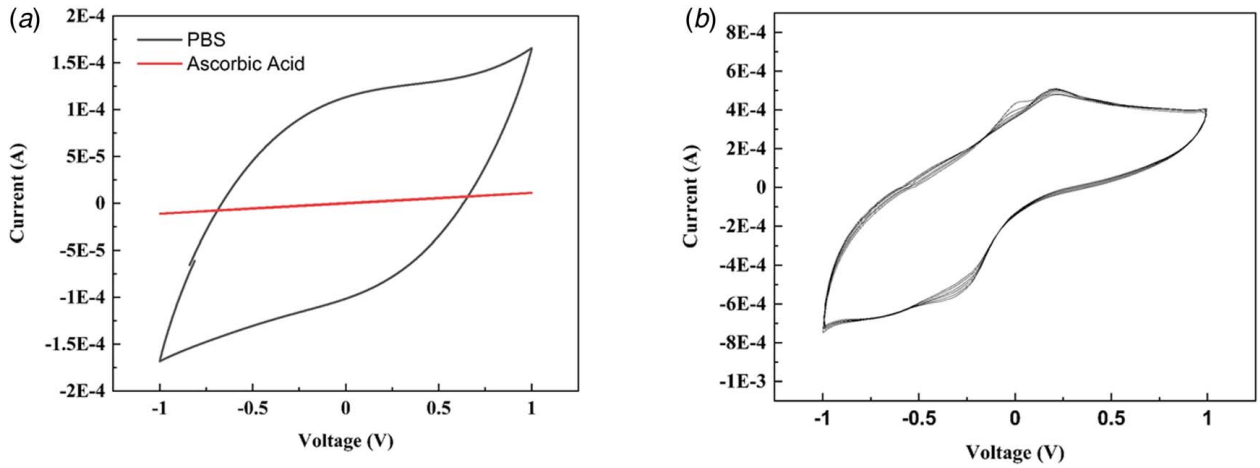

Fig. 7 CV characterization of graphene biosensor: (*a*) CV profile of 0.1 M PBS and acid ascorbic and (*b*) CV profile of 0.001 M DA at the interface of acid ascorbic using 3D-printed graphene device as the electrode

The graphene was prepared using direct liquid-phase exfoliation for the inkjet printing process. The procedure of graphene production was started by exfoliating graphite crystallites (≈20 μM). An aqueous solution of graphite and BSA was prepared in plastic containers, which then were sealed with glue and placed in metal containers. Then, a shear tension was applied to the solution using steel balls with the diameter of 11/32 in. and ½ in. at a constant rotational speed of 300 rpm. The shaking continued for 90 h to complete the exfoliation process. The ratio of the overall surface area of the balls with respect to the solution volume was kept constant for all solutions at 500 ± 10 m^2/m^3.

Raman spectroscopy was used to detect the defects on graphene ink. The ratio of I_D/I_G (D band at 1350 cm^{-1} and G band at 1590 cm^{-1}) is less than 3.5, which implies the absence of boundary and sp^3 defects in the graphene structure and emphasizes on the formation of defect-free graphene (Fig. 1(*b*)). Scanning electron microscopy (SEM) analysis was used to investigate the morphology of the printed electrodes. The absence of voids on the print surface shows the uniformity of printed electrodes. The SEM images reveal the production of connected lines in the e-jet process in a micron scale at different processing parameters (Fig. 1(*a*)).

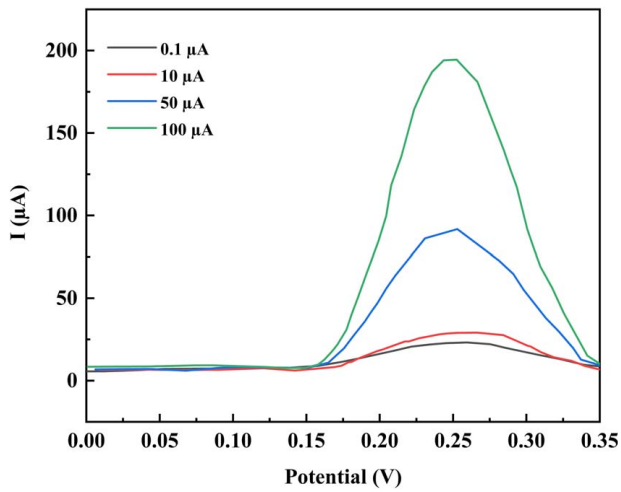

Fig. 8 DPV results of graphene biosensors at different concentrations of dopamine in the presence of 0.1 M PBS at pH = 7

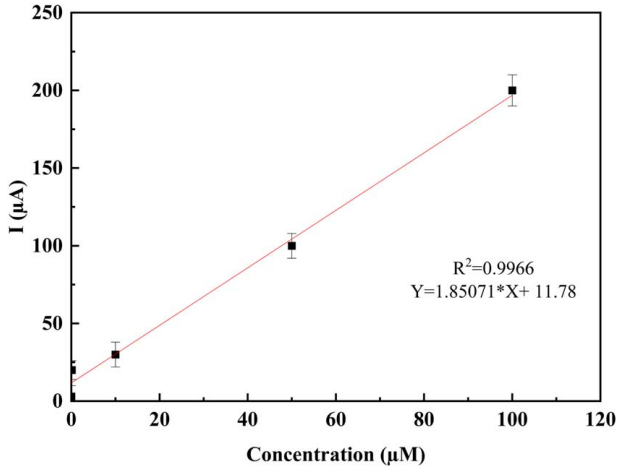

Fig. 9 The response of biosensor to different concentrations of dopamine

Electrohydrodynamic-jet (e-jet) printing utilizes a high-voltage difference between electrically conductive nozzles. There are different processing parameters that can control the final properties of graphene electrodes. Based on our previous study, the following parameters were selected to measure the conductivity of final sensor, including nozzle speed of 300 mm/min, voltage of 1 kV, and flowrate of 15 μL/min.

E-jet printing technique enables the production of a high-resolution printing of graphene electrodes. Therefore, the finger spacing can be decreased to confine the interaction of cells with graphene biosensors.

Inkjet-printed graphene was interfaced with copper tape, and electrodes were adhered to copper using conductive silver colloidal paste to maintain and extend electrical conductivity. The cell culture canister was created by cutting 2-in. sections from 15 ml centrifuge tubes and affixing them onto the graphene interface with epoxy and PDMS to maintain biocompatibility. This PDMS was then cured at 65 °C for 3 h to prevent melting of the cell culture canister. PDMS was also cured inside the test chamber to provide a "trench" for further accuracy when interfacing the cells. The trench was created by taping a microscope slide to the cell culture canister and curing PDMS around the microscope slide inside the cell culture canister. The PDMS was cured at 65 °C for 3 h (Fig. 2).

2.3 Cell Culture and Viability Studies. N27 cells were cultured at 5% CO_2 and 37 °C. Cells were cultured in maintenance media made with RPMI 1640 media (Fisher Scientific, Waltham, MA), which was supplemented with 10% fetal bovine serum in a one-shot format (Fisher Scientific), 1% L-glutamine (200 mM (100X), Fisher Scientific), and 1% penicillin (10,000 U/ml) and streptomycin (10,000 μg/ml, Fisher Scientific). To seed cells into

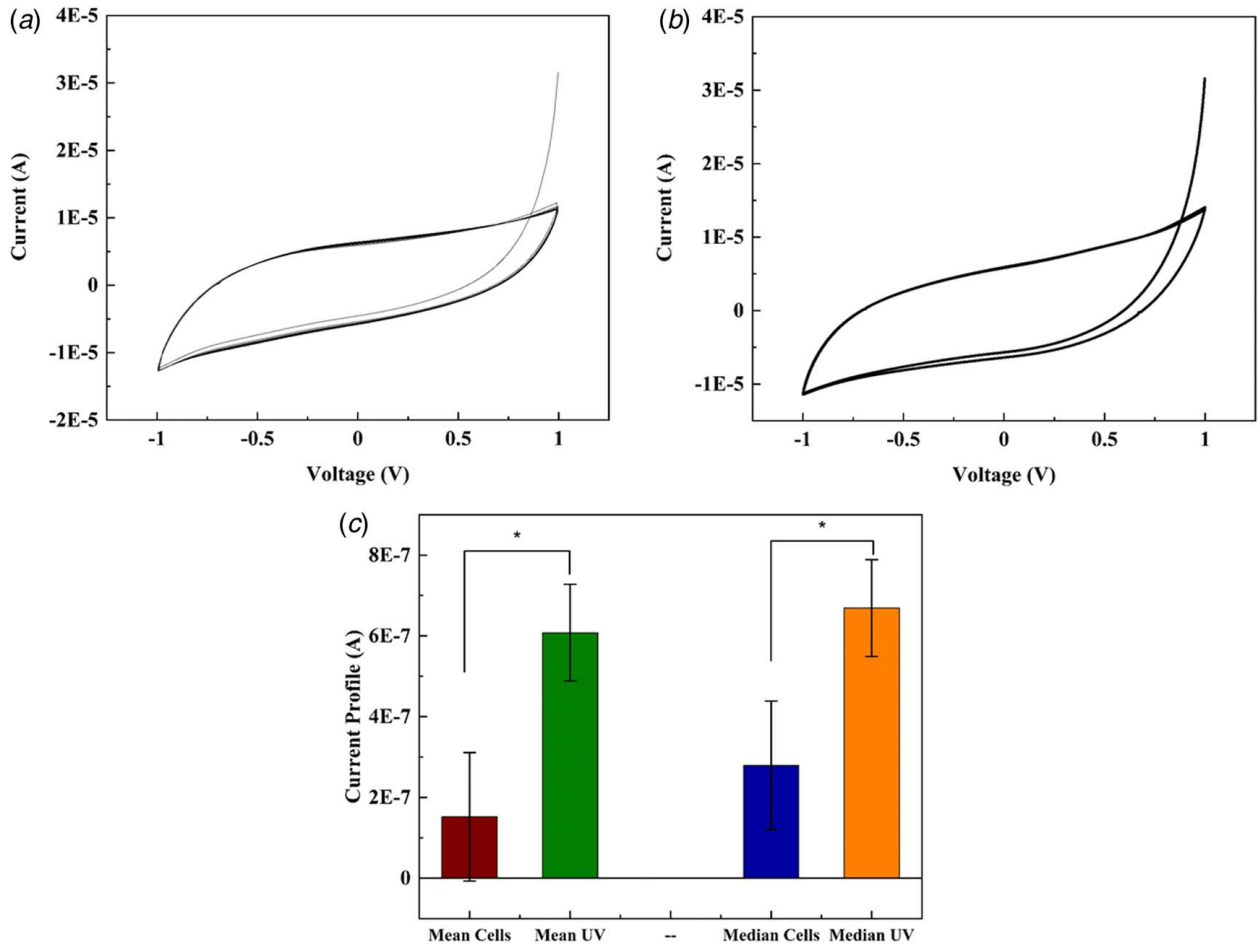

Fig. 10 Cyclic voltammetry profiles taken from live cells before and after applying the UV trauma case. The 3D-printed graphene device was the only electrode source: (*a*) cyclic voltammetry profile of live cells before UV application, (*b*) profile of live cells after UV application, and (*c*) the average and median current values shown for the two cases: before UV application and after UV application. Two-sample t-test, *p < 0.05 (results were averaged for three measurements).

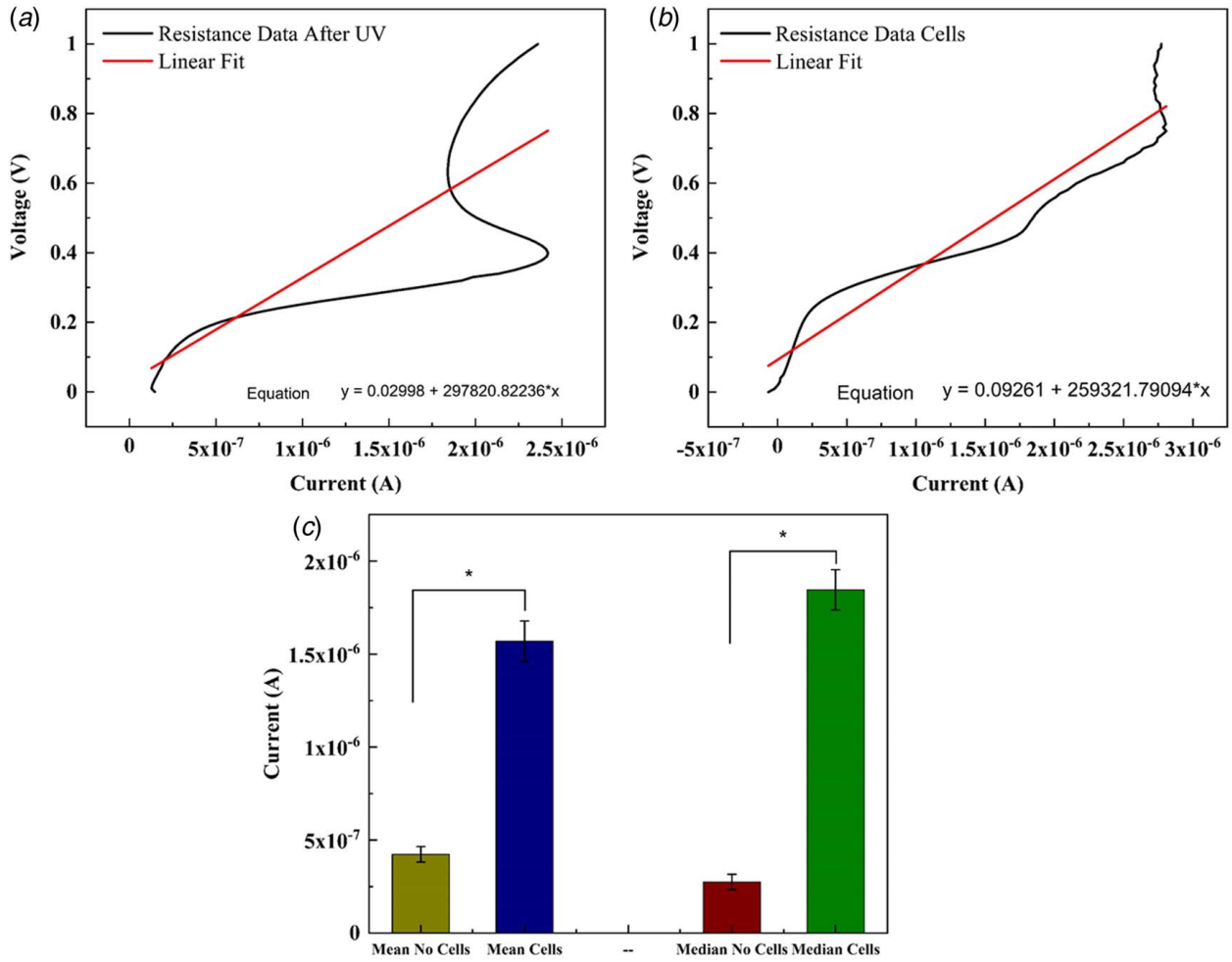

Fig. 11 (*a*) Resistance data and linear fit equation for cells cultured on the graphene device. Graphene was used as the only electrode source ($R^2 = 0.88$), (*b*) resistance data and linear fit equation after cells have been subjected to the UV trauma case ($R^2 = 0.76$), and (c) mean and median comparisons between the two cases: live cells cultured on the device and UV trauma case applied. *p > 0.05. Results were averaged for three measurements.

the sensor, 1.5 ml of maintenance media was introduced into the cell canister, and 75 μL of a 1.53×10^6 cell/ml suspension was introduced into the trench. Cells were interfaced with the 3D-printed graphene sensor using standard cell passaging protocols. A total of 0.25% trypsin-EDTA (Fisher Scientific) was used to perform cell passaging. All testing was performed at 24 h of incubation.

All cell staining was performed using 25 μM CellTracker™ Green CMFDA (Invitrogen, Carlsbad, CA) and 80 μM propidium iodide to evaluate the biocompatibility of the sensors. Cells were first rinsed using 500 μL of RPMI 1640 FBS free media. Cell staining solution (500 μL) was then administered to the cells. Cells were incubated at 5% CO_2 and 37 °C for 24 min after applying cell staining solution and rinsed twice after incubation using of FBS free RPMI 1640 media (500 μL). Imaging was performed using the 6D acquisition feature on the Zeiss Observer optical microscope.

2.4 Electrochemistry. Dopamine hydrochloride in a powder form (molecular weight 189.64 g/mol) was purchased from Sigma-Aldrich. Dopamine solutions were obtained by dissolving the necessary amounts of dopamine in 0.1 M PBS. PBS tablets were purchased from Fisher Scientific. The PBS solution was created by dissolving one tablet in 20 ml of DI water to obtain a 0.1 M solution.

Resistance, cyclic voltammetry, and staircase linear scan voltammetry testing were performed using the VersaStat 4 potentiostat (Ametek, Inc., Berwyn, PA) and a Keysight 34410A 6.5 digital multimeter (Keysight, Santa Rosa, CA). For cyclic voltammetry, trials were run from −1 V to 1 V with a scan rate of 1 V/s.

3 Results and Discussion

3.1 Biocompatibility Analysis and Live-Dead Cell Assays. The 3D-printed graphene device was printed on the Kapton substrate, and the conductivity of electrodes was investigated before the cell culture step to minimize the error associated with discontinuity of the prints. Figure 3 shows the fabrication stages of the sensor design for characterizing dopamine and trauma in dopaminergic neurons. The graphene electrodes were printed on Kapton substrate attached to glass slides. Then, the printed sensor was peeled off from glass slides after drying of electrodes in oven. The flexibility of the sensor was proven by preserving the conductivity under loading (Fig. 3(*a*)), which makes these sensors applicable in healthcare electronics.

Figure 4 shows that cellular viability was maintained after introducing the cells to the 3D-printed graphene device. Cells were introduced to the sensor using a volume of 75 μL and a concentration of 1.5×10^6 cells/ml. Live-dead cell assays were conducted after 24 h of incubation. The live cells are colored in green, and the red color shows the dead cells. The live-dead cell assay was investigated using a Zeiss Axio Observer Z1 inverted microscope that can collect green excitation/emission spectra related to CellTracker™ CMFDA and red excitation/emission spectra for propidium

iodide. The viability of cells can be calculated using the following equation:

$$\text{Viability} = \frac{\text{Live cells (green)}}{\text{Live cells (green)} + \text{Dead cells (red)}} \times 100 \quad (1)$$

Since the high biocompatibility is vital for long-term and stable cellular interfaces, as well as tissue interfaces [42] and can be used in applications such as tissue engineering and drug delivery, this is important to perform biocompatibility tests on graphene sensors.

Figure 5 shows the percentage of live cells on chip compared to the control well. Figure 5 also shows that the 90% of live cells of control well change to 85% of live cells by interfacing the cells on graphene biosensors. The results prove that the mechanically exfoliated graphene offers excellent biocompatibility, showing only 11 nonviable cells in one image of an inkjet-printed graphene line, and 6 nonviable cells in an optical image of another inkjet-printed graphene line in a 1 mm^2 space.

Recently, Hong et al. demonstrated that graphene exerts fewer adverse effects on neural cells than single-wall carbon nanotubes and multiwall carbon nanotubes, not showing any adverse effects on PC12 neurons until a concentration of 62.5 ppm was reached [43]. Reactive oxidative species, cell proliferation, and metabolic activity were investigated. Also, PC12 cell proliferation was enhanced in the presence of fetal bovine serum (FBS)-covered graphene [7]. However, graphene was prepared using chemical vapor deposition in this work [43], and the biocompatibility of wet milled, mechanically exfoliated graphene with BSA added for further exfoliation was not investigated. Rastogi et al. demonstrated that graphene has no detectable adverse effects on mitochondrial membrane potential and morphology. The group demonstrated this on nonneuronal and neuronal cell lines [44]. However, graphene in this study was again prepared using chemical vapor deposition, and further investigation on mechanically exfoliated graphene with BSA for possible improvements in biocompatibility and validation of biocompatibility is necessary [44].

3.2 Cyclic Voltammetry Characterization. Cyclic voltammetry was used with the 3D-printed graphene device to characterize 1 mM dopamine solutions (Fig. 6). Dopamine solutions were prepared by dissolving dopamine hydrochloride powder in 0.1 M PBS. The graphene device was used as the only electrode source.

We then sought to characterize the dopamine output from the N27 dopaminergic neurons using the 3D-printed graphene device as the only electrode source. Cells were seeded on to the graphene device using a volume of 19 μL at a concentration of 1.53×10^6 cells/ml. Cells were analyzed after at least 24 h, and studies reported here were undertaken after 72 h (Fig. 7(*a*)). Cyclic voltammetry was used to investigate the dopamine output from the N27 and to

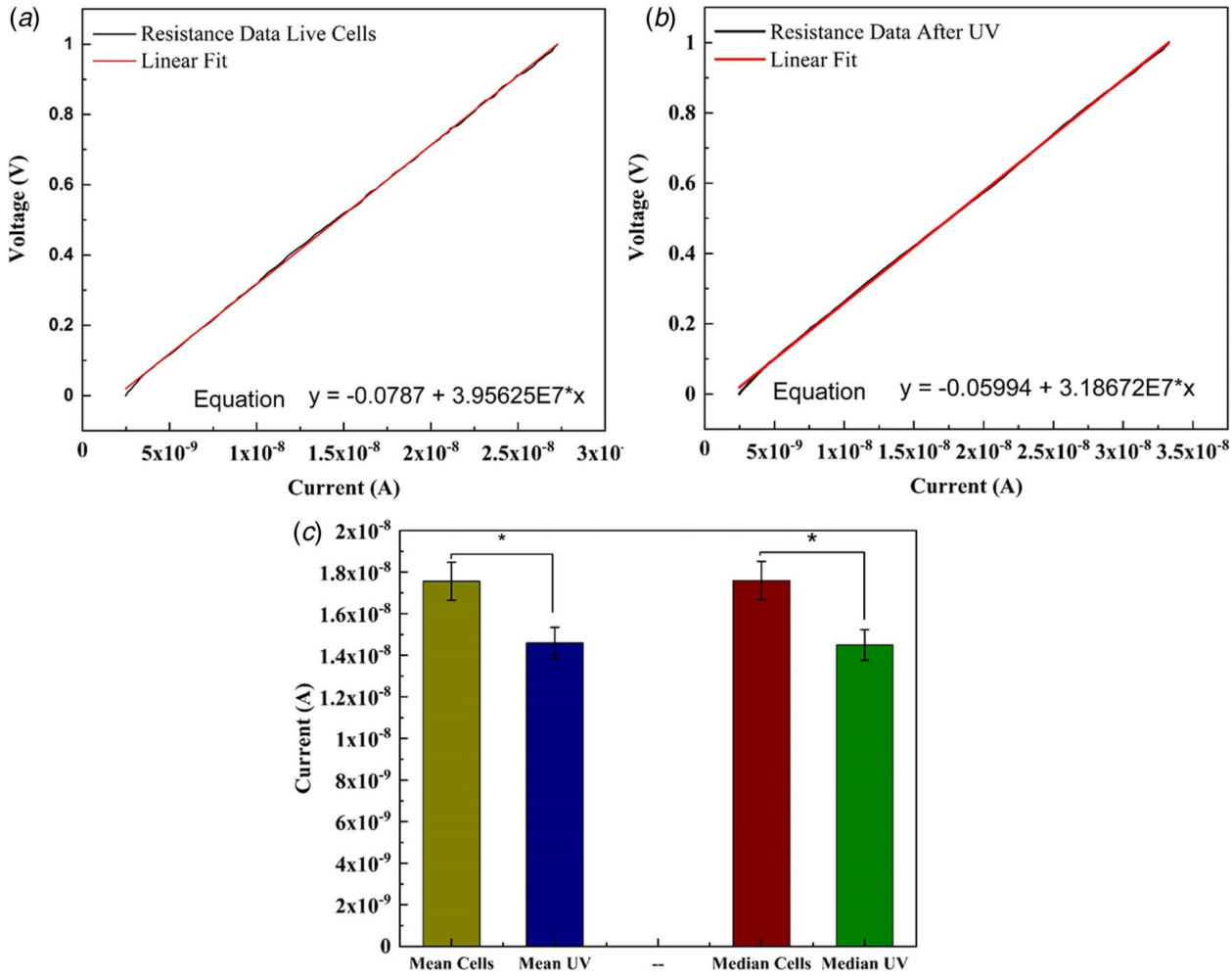

Fig. 12 (*a*) Resistance data and linear fit equation for cells cultured on the graphene device. Graphene was used as the only electrode source ($R^2 = 0.99$), (*b*) resistance data and linear fit equation after cells have been subjected to the UV trauma case ($R^2 = 0.99$), and (*c*) mean and median comparisons between the two cases: live cells cultured on the device and UV trauma case applied. *p > 0.05. Results were averaged for three measurements.

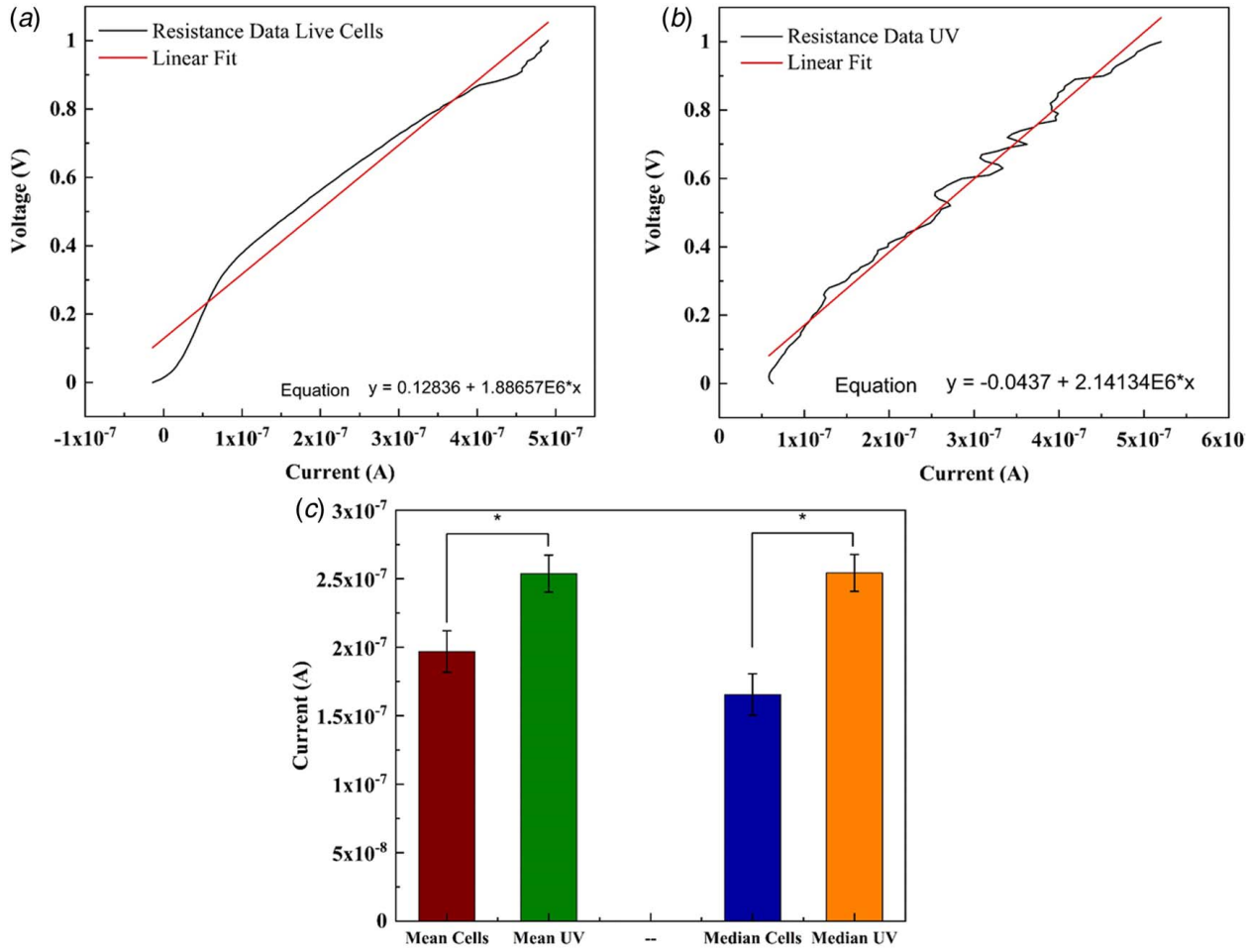

Fig. 13 (*a*) Resistance data and linear fit equation for cells cultured on the graphene device. Graphene was used as the only electrode source, $R^2 = 092$, (*b*) resistance data and linear fit equation after cells have been subjected to the UV trauma case, $R^2 = 0.90$, and (c) mean and median comparisons between the two cases: live cells cultured on the device and UV trauma case applied. *p > 0.05. Results were averaged for three measurements.

compare the results to the dopamine solution (Fig. 7(*a*)). We then sought to compare these profiles to the data gathered after the cells were exposed to trauma (Fig. 9). To cause damage and not a loss in viability, cells were exposed to UV radiation for 20 s. It has been previously shown by Nakata et al. [45] that light energy can cause neural degeneration as invasive lesion techniques. Irradiation of UV light induced a focal brain lesion, and the damage depends on the amount of UV exposure. The purpose of UV irradiation is to generate damage to cells using UV light and study the change of neural circuits in exposure to UV as the neural degenerative stimulant.

The cyclic voltammetry profile was taken and then compared with the nontrauma case (Fig. 10) with the calculation of standard errors, and the experiments were repeated for three samples in each experiment. Similarly, the N27 cells were cultured on the device and the resistance of the graphene was measured using staircase linear scan voltammetry. Linear sweeps were performed from 0 V to 1 V with a step size of 0.1 V, and the resulting current was measured. The cells cultured on the device were then exposed to 20 s of UV radiation to induce damage, and the resulting resistance was again measured using staircase linear scan voltammetry and the same parameters. These results are shown in Figs. 11–13. The statistical significance was calculated using a two-sample t-test.

According to Fig. 6, the CV analysis of 0.001 M DA using graphene electrodes shows one oxidation peak at 0.25 V and one reduction peak at −0.25 V. These values show the quasi-reversible behavior of graphene electrodes to redox reaction of dopamine. Figures 6(*a*) and 6(*b*) compare the functionality of biosensors with different processing conditions. The processing condition of the graphene electrode shown in Fig. 6(*a*) was used for the fabrication of biosensors presented here in this work.

The oxygen-containing functional groups on the surface of graphene would selectively absorb dopamine through the π-π interactions between phenyl groups on dopamine and graphene carbons. There are other interfering neurotransmitters like ascorbic acids and glucose in the human body, and the detection of dopamine using graphene sensors in the presence of interfering compounds should be examined. The selectivity of the graphene electrodes was evaluated at the interface of ascorbic acid. The variation of current as a result of adding dopamine and ascorbic acid is shown in Fig. 7. Figure 7(*a*) shows that the current change in 0.1 M PBS has no indication of oxidation and reduction peaks.

The current shows a significant change in the current by adding dopamine, while there is no significant change in the current variation by including ascorbic acid in our solution. Based on Fig. 7, the graphene surface may repel the negatively charged groups of ascorbic acid as it does not provide a significant change in the biosensor current. According to Fig. 7(*b*), a small peak at −0.58 V can be seen, which is related to ascorbic acid. The comparison between Figs. 6(*a*) and 7(*b*) shows that the acid ascorbic did not change the detection capability of the biosensor implying a good selectivity of graphene biosensors and the peaks related to dopamine did not change in the presence of ascorbic acid.

To evaluate the sensitivity of graphene biosensor to different concentrations of dopamine, differential pulse voltammetric analysis

(DPV) was performed. DPV measurement showed that the solution consists of 0.1 M PBS at pH = 7 and dopamine in the potential range of 0–0.4 V at an amplitude of 0.025 V, a step potential of 0.05 V, and a scan rate of 50 mV/s (Fig. 8).

We can calculate the limit of detection (LOD) using the following equation [9]:

$$\text{LOD} = \frac{3S}{q} \tag{2}$$

where q is the slope of calibration curve and S is the standard deviation. The response of dopamine has a linear relationship between dopamine concentration and current. According to Fig. 9, the correlation coefficient is 0.9966, and the LOD was measured to be 180 μ, which shows a good sensitivity of a graphene biosensor in detection of dopamine within the dynamic range of 0.1–100 μM.

The novel, 3D-printed, mechanically exfoliated, biocompatible graphene system was the only electrode source. It can be seen that the trauma case provided a significant difference in the current profiles over the course of the cyclic voltammetry tests (Fig. 9).

According to Fig. 10, UV exposure caused cell detachment of neural cells and increased the current passing through the graphene electrodes. Similarly, the generated circuit by including cells into graphene sensors creates an insulator layer of cells [46] that increased the resistance of the sensor, and after UV irradiation, cells will detach from the graphene electrodes, and the average of resistance decreased compared to having live cells between electrodes (Figs. 11–13).

The results were consistent with literature findings, which validates the 3D-printed graphene sensor described in this article [44,47]. As mentioned earlier, CV has been used to measure dopamine using graphene-based electrodes and electrochemical systems [3,48–52]. We provide cyclic voltammetry characterization of prepared dopamine solutions consistent with Gilhane et al. [47].

We also demonstrated a change in the cyclic voltammetry profile taken, while live cells were cultured on the 3D-printed graphene device.

3.3 Cyclic Voltammetry Data Analysis. As suggested by Chemistry libre texts, the electrode potential can be characterized as follows:

$$E = E_i + vt \tag{3}$$

where E_i is the initial potential in volts, v is the sweep rate in volts per second, and t is the time in seconds. As the parameters in this study were as follows: $E_i = -1$ V, $v = 1$ V/s, and $t = 4$ s, it can be found that the potential of the 3D-printed graphene device used as an electrode at the time of characterization was approximately 3 V (Eq. (1)). This can also be represented using the following equation to obtain the same result when the direction of the potential sweep is switched:

$$E = E_s - vt \tag{4}$$

where E_s is the potential at the switching point, given as 1 V in this study (Eq. (2)).

The formal reduction potential ($E^{\circ\prime}$) can also be calculated and is the mean of E_{pc} and E_{pa} values:

$$E^{\circ\prime} = \frac{E_{pa} + E_{pc}}{2} \tag{5}$$

where E_{pa} is the peak anodic peak potential and E_{pc} is the cathodic peak potential. Figure 5 shows that E_{pa} is approximately −0.3 V and E_{pc} is approximately 0.25 V. It can then be seen that $E^{\circ\prime}$ is approximately −0.025 V (Eq. (3)). The pH of the solution tested was found to be 7.01 via a pH meter (Thermo Fisher Scientific, Waltham, MA). Krampa et al. recorded E_{pa} to be 0.328 V and E_{pc} to be 0.299 V using graphene nanoplatelet electrodes [53].

4 Conclusions

In this study, we fabricated 3D-printed graphene electrodes, being one of the first studies to use these 3D-printed electrodes to characterize dopamine release. Preliminary steps involved demonstrating the biocompatibility of the device using live-dead cell assays via CellTracker™ Green CMFDA and propidium iodide.

Prepared dopamine solutions were characterized via cyclic voltammetry using the 3D-printed graphene device, and the peak cathodic current was consistent with the graphene electrode device that was used to measure dopamine levels in literature [53]. We demonstrated that the device is able to exhibit peak voltages when running cyclic voltammetry tests to characterize dopamine solutions. This paves the way for further electrochemical characterization using the device interfaced with dopaminergic neurons, as well as the potential of the device to measure ion channel flow in dopaminergic neurons.

Finally, we used this novel, mechanically exfoliated, and 3D-printed graphene device to characterize damage to the dopaminergic neurons in the face of trauma. UV trauma was applied, and the cyclic voltammetry results taken from live cells after applying trauma showed significant differences from those taken before trauma was applied. This is crucial in lending understanding to the field of traumatic brain injury and characterizing trauma in cellular systems.

Acknowledgment

This work was partially supported by the Office of Naval Research Grant N000141712620 and National Science Foundation Award 2014346. The authors would like to acknowledge Dr. Kanthasamy for the generous gift of the N27 dopaminergic neurons and Dr. Donald Sakaguchi for his technical assistance and constructive discussions.

Conflict of Interest

There are no conflicts of interest.

Data Availability Statement

The datasets generated and supporting the findings of this article are obtainable from the corresponding author upon reasonable request.

References

[1] Senel, M., Dervisevic, M., Alhassen, S., Alachkar, A., and Voelcker, N. H., 2020, "Electrochemical Micropyramid Array-Based Sensor for In Situ Monitoring of Dopamine Released From Neuroblastoma Cells," Anal. Chem., **92**(11), pp. 7746–7753.

[2] Jolly, A. E., Raymont, V., Cole, J. H., Whittington, A., Scott, G., De Simoni, S., Searle, G., Gunn, R. N., and Sharp, D. J., 2019, "Dopamine D2/D3 Receptor Abnormalities After Traumatic Brain Injury and Their Relationship to Post-Traumatic Depression," Neuroimage Clin., **24**, p. 101950.

[3] Ben Ali Hassine, C., Kahri, H., and Barhoumi, H., 2020, "Enhancing Dopamine Detection Using Glassy Carbon Electrode Modified With Graphene Oxide, Nickel and Gold Nanoparticles," J. Electrochem. Soc., **167**(2), p. 027516.

[4] Suzuki, I., Fukuda, M., Shirakawa, K., Jiko, H., and Gotoh, M., 2013, "Carbon Nanotube Multi-Electrode Array Chips for Noninvasive Real-Time Measurement of Dopamine, Action Potentials, and Postsynaptic Potentials," Biosens Bioelectron., **49**, pp. 270–275.

[5] Lan, Y. L., Li, S., Lou, J. C., Ma, X. C., and Zhang, B., 2019, "The Potential Roles of Dopamine in Traumatic Brain Injury: A Preclinical and Clinical Update," Am. J. Transl. Res., **11**(5), pp. 2616–2631.

[6] Cannella, L. A., Andrews, A. M., Tran, F., Razmpour, R., McGary, H., Collie, C., Tsegaye, T., Maynard, M., Kaufman, M.J., Rawls, S.M., and Ramirez, S.H., 2020, "Experimental Traumatic Brain Injury During Adolescence Enhances Cocaine Rewarding Efficacy and Dysregulates Dopamine and Neuroimmune Systems in Brain Reward Substrates," J. Neurotrauma, **37**(1), pp. 27–42.

[7] Rosas-Hernandez, H., Burks, S. M., Cuevas, E., and Ali, S. F., 2019, "Stretch-Induced Deformation as a Model to Study Dopaminergic Dysfunction in Traumatic Brain Injury," Neurochem. Res., **44**(11), pp. 2546–2555.

[8] Fridman, E. A., Osborne, J. R., Mozley, P. D., Victor, J. D., and Schiff, N. D., 2019, "Presynaptic Dopamine Deficit in Minimally Conscious State Patients Following Traumatic Brain Injury," Brain, **142**(7), pp. 1887–1893.
[9] Arumugasamy, S. K., Govindaraju, S., and Yun, K., 2020, "Electrochemical Sensor for Detecting Dopamine Using Graphene Quantum Dots Incorporated With Multiwall Carbon Nanotubes," Appl. Surf. Sci., **508**, p. 145294.
[10] Diab, N., Morales, D. M., Andronescu, C., Masoud, M., and Schuhmann, W., 2019, "A Sensitive and Selective Graphene/Cobalt Tetrasulfonated Phthalocyanine Sensor for Detection of Dopamine," Sens. Actuators, B, **285**, pp. 17–23.
[11] Huang, Q. T., Lin, X. F., Tong, L. L., and Tong, Q. X., 2020, "Graphene Quantum Dots/Multiwalled Carbon Nanotubes Composite-Based Electrochemical Sensor for Detecting Dopamine Release From Living Cells," ACS Sustain. Chem. Eng., **8**(3), pp. 1644–1650.
[12] Liao, C. Z., Zhang, M., Niu, L. Y., Zheng, Z. J., and Yan, F., 2014, "Organic Electrochemical Transistors With Graphene-Modified Gate Electrodes for Highly Sensitive and Selective Dopamine Sensors," J. Mater. Chem. B, **2**(2), pp. 191–200.
[13] Kujawska, M., Bhardwaj, S. K., Mishra, Y. K., and Kaushik, A., 2021, "Using Graphene-Based Biosensors to Detect Dopamine for Efficient Parkinson's Disease Diagnostics," Biosensors, **11**(11), p. 433.
[14] Hou, S. F., Kasner, M. L., Su, S. J., Patel, K., and Cuellari, R., 2010, "Highly Sensitive and Selective Dopamine Biosensor Fabricated With Silanized Graphene," J. Phys. Chem. C, **114**(35), pp. 14915–14921.
[15] Qi, S. P., Zhao, B., Tang, H. Q., and Jiang, X. Q., 2015, "Determination of Ascorbic Acid, Dopamine, and Uric Acid by a Novel Electrochemical Sensor Based on Pristine Graphene," Electrochim. Acta, **161**, pp. 395–402.
[16] Darwish, L. R., El-Wakad, M. T., and Farag, M. M., 2021, "Towards an Ultra-Affordable Three-Dimensional Bioprinter: A Heated Inductive-Enabled Syringe Pump Extrusion Multifunction Module for Open-Source Fused Deposition Modeling Three-Dimensional Printers," ASME J. Manuf. Sci. Eng., **143**(12), p. 125001.
[17] Jin, Y., Xiong, R., Antonelli, P. J., Long, C. J., McAleer, C. W., Hickman, J. J., and Huang, Y., 2021, "Nanoclay Suspension-Enabled Extrusion Bioprinting of Three-Dimensional Soft Structures," ASME J. Manuf. Sci. Eng., **143**(12), p. 121004.
[18] Choo, S. S., Kang, E. S., Song, I., Lee, D., Choi, J. W., and Kim, T. H., 2017, "Electrochemical Detection of Dopamine Using 3D Porous Graphene Oxide/Gold Nanoparticle Composites," Sensors, **17**(4), p. 861.
[19] Pemathilaka, R. L., Caplin, J. D., Aykar, S. S., Montazami, R., and Hashemi, N. N., 2019, "Placenta-on-a-Chip: In Vitro Study of Caffeine Transport Across Placental Barrier Using Liquid Chromatography Mass Spectrometry," Glob. Chall., **3**(3), p. 1800112.
[20] Caplin, J. D., Granados, N. G., James, M. R., Montazami, R., and Hashemi, N., 2015, "Microfluidic Organ-on-a-Chip Technology for Advancement of Drug Development and Toxicology," Adv. Healthcare Mater., **4**(10), pp. 1426–1450.
[21] Bai, Z., Mendoza Reyes, J. M., Montazami, R., and Hashemi, N., 2014, "On-Chip Development of Hydrogel Microfibers From Round to Square/Ribbon Shape," J. Mater. Chem. A, **2**(14), pp. 4878–4884.
[22] Hashemi, N., Lackore, J. M., Sharifi, F., Goodrich, P. J., Winchell, M. L., and Hashemi, N., 2016, "A Paper-Based Microbial Fuel Cell Operating Under Continuous Flow Condition," Technology, **4**(2), pp. 98–103.
[23] Acar, H., Çınar, S., Thunga, M., Kessler, M. R., Hashemi, N., and Montazami, R., 2014, "Study of Physically Transient Insulating Materials as a Potential Platform for Transient Electronics and Bioelectronics," Adv. Funct. Mater., **24**(26), pp. 4135–4143.
[24] Sharifi, F., Patel, B. B., McNamara, M. C., Meis, P. J., Roghair, M. N., Lu, M., Montazami, R., Sakaguchi, D. S., and Hashemi, N. N., 2019, "Photo-Cross-Linked Poly(Ethylene Glycol) Diacrylate Hydrogels: Spherical Microparticles to Bow Tie-Shaped Microfibers," ACS Appl. Mater. Interfaces, **11**(20), pp. 18797–18807.
[25] Sharifi, F., Patel, B. B., Dzuilko, A. K., Montazami, R., Sakaguchi, D. S., and Hashemi, N., 2016, "Polycaprolactone Microfibrous Scaffolds to Navigate Neural Stem Cells," Biomacromolecules, **17**(10), pp. 3287–3297.
[26] Sechi, D., Greer, B., Johnson, J., and Hashemi, N., 2013, "Three-Dimensional Paper-Based Microfluidic Device for Assays of Protein and Glucose in Urine," Anal. Chem., **85**(22), pp. 10733–10737.
[27] Niaraki, A., Abbasi Shirsavar, M., Aykar, S. A., Taghavimehr, M., Montazami, R., and Hashemi, N., 2022, "Minute-Sensitive Real-Time Monitoring of Neural Cells Through Printed Graphene Microelectrodes," Biosens. Bioelectron., **210**, p. 114284.
[28] Chen, R., Chang, R. C., Tai, B., Huang, Y., Ozdoganlar, B., Li, W., and Shih, A., 2020, "Biomedical Manufacturing: A Review of the Emerging Research and Applications," ASME J. Manuf. Sci. Eng., **142**(11), p. 110807.
[29] Thakare, K., Jerpseth, L., Qin, H., and Pei, Z., 2021, "Bioprinting Using Algae: Effects of Extrusion Pressure and Needle Diameter on Cell Quantity in Printed Samples," ASME J. Manuf. Sci. Eng., **143**(1), p. 014501.
[30] Manbohi, A., and Ahmadi, S. H., 2019, "Sensitive and Selective Detection of Dopamine Using Electrochemical Microfluidic Paper-Based Analytical Nanosensor," Sens. Bio-Sens. Res., **23**, p. 100270.
[31] Zhao, J., Zhao, L., Lan, C., and Zhao, S., 2016, "Graphene Quantum Dots as Effective Probes for Label-Free Fluorescence Detection of Dopamine," Sens. Actuators, B, **223**, pp. 246–251.
[32] Shirsavar, M. A., Taghavimehr, M., Ouedraogo, L. J., Javaheripi, M., Hashemi, N. N., Koushanfar, F., and Montazami, R., 2021, "Machine Learning-Assisted E-jet Printing of Organic Flexible Biosensors," arXiv.
[33] De Alwis, S., Abbasi Shirsavar, M., Singh, S., and Hashemi, N. N., 2021, "Hydrodynamic Cavitation for Scalable Exfoliation of Few-Layered Graphene Nanosheets," Nanotechnology, **32**(50), p. 505701.
[34] Clarke, G. A., Hartse, B. X., Niaraki Asli, A. E., Taghavimehr, M., Hashemi, N., Abbasi Shirsavar, M., Montazami, R., Alimoradi, N., Nasirian, V., Ouedraogo, L.J., and Hashemi, N.N., 2021, "Advancement of Sensor Integrated Organ-on-Chip Devices," Sensors, **21**(4).
[35] Guo, J., Niaraki Asli, A. E., Williams, K. R., Lai, P. L., Wang, X., Montazami, R., and Hashemi, N. N., 2019, "Viability of Neural Cells on 3D Printed Graphene Bioelectronics," Biosensors, **9**(4), p. 112.
[36] Anuar, N. S., Basirun, W. J., Shalauddin, M., and Akhter, S., 2020, "A Dopamine Electrochemical Sensor Based on a Platinum–Silver Graphene Nanocomposite Modified Electrode," RSC Adv., **10**(29), pp. 17336–17344.
[37] Lee, T. H., Fan, H.-T., Li, Y., Shriver, D., Arinez, J., Xiao, G., and Banu, M., 2020, "Enhanced Performance of Ultrasonic Welding of Short Carbon Fiber Polymer Composites Through Control of Morphological Parameters," ASME J. Manuf. Sci. Eng., **142**(1), p. 011009.
[38] Wu, B., Hassanein, A., Wang, M., Tripathi, J. K., and Kang, Z., 2020, "Laser-Based Fabrication of Carbon Nanotube–Metal Composites on a Polymer Substrate: Experimental Study and Characterizations," ASME J. Manuf. Sci. Eng., **142**(9), p. 091007.
[39] Emran, M. Y., Shenashen, M. A., Morita, H., and El-Safty, S. A., 2018, "3D-Ridge Stocked Layers of Nitrogen-Doped Mesoporous Carbon Nanosheets for Ultrasensitive Monitoring of Dopamine Released From PC12 Cells Under K(+) Stimulation," Adv. Healthc. Mater., **7**(16), p. e1701459.
[40] Niaraki Asli, A. E., Guo, J., Lai, P. L., Montazami, R., and Hashemi, N. N., 2020, "High-Yield Production of Aqueous Graphene for Electrohydrodynamic Drop-on-Demand Printing of Biocompatible Conductive Patterns," Biosensors, **10**(1), p. 6.
[41] McNamara, M. C., Niaraki-Asli, A. E., Guo, J., Okuzono, J., Montazami, R., and Hashemi, N. N., 2020, "Enhancing the Conductivity of Cell-Laden Alginate Microfibers With Aqueous Graphene for Neural Applications," Front. Mater., **7**.
[42] Rastogi, S. K., Bliley, J., Matino, L., Garg, R., Santoro, F., Feinberg, A. W., and Cohen-Karni, T., 2020, "Three-Dimensional Fuzzy Graphene Ultra-Microelectrodes for Subcellular Electrical Recordings," Nano Res., **13**(5), pp. 1444–1452.
[43] Hong, S. W., Lee, J. H., Kang, S. H., Hwang, E. Y., Hwang, Y. S., Lee, M. H., Han, D. W., and Park, J. C., 2014, "Enhanced Neural Cell Adhesion and Neurite Outgrowth on Graphene-Based Biomimetic Substrates," Biomed. Res. Int., **2014**, p. 212149.
[44] Rastogi, S. K., Raghavan, G., Yang, G., and Cohen-Karni, T., 2017, "Effect of Graphene on Nonneuronal and Neuronal Cell Viability and Stress," Nano Lett., **17**(5), pp. 3297–3301.
[45] Nakata, M., Nagasaka, K., Shimoda, M., Takashima, I., and Yamamoto, S., 2018, "Focal Brain Lesions Induced With Ultraviolet Irradiation," Sci. Rep., **8**, p. 7968 .
[46] Niaraki, A., McNamara, M. C., Montazami, R., and Hashemi, N. N., 2022, "Graphene Microelectrodes for Real-Time Impedance Spectroscopy of Neural Cells," ACS Appl. Bio. Mater., **5**(1), pp. 113–122.
[47] Ghilane, J., Hapiot, P., and Bard, J., 2006, "Metal/Polypyrrole Quasi-Reference Electrode for Voltammetry in Nonaqueous and Aqueous Solutions," Anal. Chem., **78**(19), pp. 6868–6872.
[48] Gunasekaran, S., Raveendran, J., Suneesh, S. P., and Babu, T., 2019, "Fabrication of Disposable Electrochemicaln Dopamine Sensor Using Photoluminescent Graphene Oxide," IOP Conf. Ser. Mater. Sci. Eng., **577**(1), p. 012105.
[49] Pampaloni, N. P., Lottner, M., Giugliano, M., Matruglio, A., D'Amico, F., Prato, M., Garrido, J. A., Ballerini, L., and Scaini, D., 2018, "Single-Layer Graphene Modulates Neuronal Communication and Augments Membrane Ion Currents," Nat. Nanotechnol., **13**(8), pp. 755–764.
[50] Chauhan, N., Chawla, S., Pundir, C. S., and Jain, U., 2017, "An Electrochemical Sensor for Detection of Neurotransmitter-Acetylcholine Using Metal Nanoparticles, 2D Material and Conducting Polymer Modified Electrode," Biosens. Bioelectron., **89**(Pt 1), pp. 377–383.
[51] Tang, L., Du, D., Yang, F., Liang, Z., Ning, Y., Wang, H., and Zhang, G. J., 2015, "Preparation of Graphene-Modified Acupuncture Needle and Its Application in Detecting Neurotransmitters," Sci. Rep., **5**(1), p. 11627.
[52] Gunasekaran, S., Raveendran, J., Suneesh, P. V., and Satheesh Babu, T. G., 2019, "Fabrication of Disposable Electrochemical Dopamine Sensor Using Photoluminescent Graphene Oxide," IOP, Bengaluru, India, 2018, p. 012105.
[53] Krampa, F. D., Aniweh, Y., Kanyong, P., and Awandare, G. A., 2020, "Graphene Nanoplatelet-Based Sensor for the Detection of Dopamine and N-Acetyl-p-Aminophenol in Urine," Arabian J. Chem., **13**(1), pp. 3218–3225.